Remote hydrological control on crustal seismicity

Francesco Pintori (Corresponding author, francesco.pintori@ingv.it)[a,b], Enrico Serpelloni (enrico.serpelloni@ingv.it)[a], Laurent Longuevergne (laurent.longuevergne@univ-rennes1.fr)[c], Alexander Garcia-Aristizabal (alexander.garcia@ingv.it)[a], Maria Elina Belardinelli (mariaelina.belardinelli@unibo.it)[b], Licia Faenza (licia.faenza@ingv.it)[a], Lucio D'Alberto (lucio.dalberto@arpa.veneto.it)[d], Adriano Gualandi (adriano.geolandi@gmail.com)[e,f]

[a] Istituto Nazionale di Geofisica e Vulcanologia, Italy.

[b] Università di Bologna, Dipartimento di Fisica e Astronomia, Settore di Geofisica, Bologna, Italy.

[c] Geosciences Rennes, UMR CNRS 6118, Université de Rennes 1,Rennes, France.

[d] ARPA Veneto, Inland Waters Office, Padova, Italy.

[e] Department of Geological and Planetary Sciences, California Institute of Technology, Pasadena, CA, USA.

[f] Jet Propulsion Laboratory, California Institute of Technology, Pasadena, CA, USA.

Keywords: GNSS; hydrology; non-tectonic deformation; stress changes; seismicity rates; Alps

Highlights:

- Changes in terrestrial water storage modulate horizontal transient deformation
- Hydrologically-active fractures focus groundwater fluxes and pressure changes
- Pressure changes in shallow fractures cause large stress changes at seismogenic depth
- Background seismicity rates are correlated with terrestrial water content

Abstract

It is known that changes in continental water storage can produce vertical surface deformation, induce crustal stress perturbations and modulate seismicity rates. However, the degree to which local changes in terrestrial water content influence the occurrence of earthquakes remains an open problem. We show how changes in terrestrial water storage, computed for a ~1000 km^2 basin, focus deformation in a narrow zone, causing horizontal, non-seasonal displacements and modulating crustal seismicity rates. We present results from a karstic mountain range located at the edge of the Adria-Eurasia plate boundary system in northern Italy, where slow shortening rates (~1 mm/yr) are accommodated across a complex fold-and-thrust belt. The presence of geological structures with high permeabilities and of deeply rooted hydrologically-active fractures focus groundwater fluxes and pressure changes, generating transient horizontal deformation and perturbations of crustal stress up to 25 kPa at seismogenic depths. The background seismicity rates are correlated, without evident temporal delay, with the terrestrial water content in the hydrological basin. Being independent from hydraulic diffusivity, seismicity modulation is likely affected by direct stress changes on faults planes.

1. Introduction

Constant redistribution of surface loads due to continental hydrology (van Dam et al., 2001) causes measurable deformation of the Earth's surface. In particular, seasonal hydrological mass movements turned out to influence tectonic deformation of the lithosphere and modulate seismicity rates in several tectonic environments (Bettinelli et al., 2008; Craig et al., 2017). While seasonal modulation of seismicity associated with vertical loading is a known process (Bettinelli et al., 2008; Craig et al., 2017), other hydrologically-driven non-seasonal deformation, mainly acting on the horizontal components, have been more recently recognized in the peri-Adriatic region (Devoti et al., 2018; Silverii et al., 2016; Serpelloni et al., 2018). Here, dense GNSS networks and important karst aquifers are present along the seismically active Apennine and South Alpine mountain chains. The hydrological nature of these deformation signals has been suggested based on temporal correlation between geodetic displacements and precipitation or spring discharge data (Hainzl et al., 2006; D'Agostino et al., 2018). Measurements of groundwater contents are not available because of the lack of water wells in mountainous regions; however, the Gravity Recovery and Climate Experiment (GRACE) can provide complementary independent observations of total water mass, but with a coarse spatial resolution (greater than scales of 300 km; Famiglietti et al., 2011). Changes in groundwater levels in karst aquifers, or fractures associated with karst systems, are considered the most likely mechanisms to explain the observed deformation, which is characterized by larger displacements in the horizontal components than in the vertical one (Devoti et al., 2015; Serpelloni et al., 2018).

Identifying and extracting non-tectonic signals from geodetic measurements remains critical to detect potential tectonic signals of small amplitude and to improve the accuracy and precision of interseismic deformation estimates. Moreover, studying hydrological deformation signals can provide new clues on elastic (Chanard et al., 2014; Drouin et al., 2016) and viscoelastic (Chanard et al., 2018) properties of the Earth, on continental water storage fluctuations (Borsa et al., 2014; Fu et al., 2013) and on the possible relationship between hydrologically-driven stress changes and earthquake nucleation. Two mechanisms by which hydrology can modulate earthquake occurrence have been suggested: variations in pore-fluid pressure at hypocentral depths (Hainzl et al., 2006) and direct stress on the fault plane (Bettinelli et al., 2008; Craig et al., 2017; Johnson et al., 2017; D'Agostino et al., 2018). An effective way to discriminate between these two processes is the presence of a time lag between hydrological indicators and seismicity rates. In fact, while the effect of the direct stress can be considered instantaneous, hydraulic diffusivity at hypocentral depth determine a time lag between hydrological and seismological indicators, if pore-fluid pressure variations are the main driver of earthquake rates modulation.

In this work we study a segment of the Adria-Eurasia plate boundary in North-Eastern Italy (Fig. 1), where ~70% of the plate convergence is presently accommodated across a south-vering fold-and-thrust belt (Serpelloni et al., 2016; Anderlini et al., 2020). The main thrusts are, from the internal parts to the foreland, the Valsugana thrust, the Belluno thrust and the Bassano-Valdobbiadene thrust (BVT), the latter being associated with a morphological relief of ~1200 m above the plain, known as Pedemountain flexure (Fig. 1). The southernmost active front is now mainly buried beneath the alluvial deposits of the Venetian plain and sealed by Late Miocene to Quaternary (~7–2.5 Ma) deposits (Fantoni et al., 2002), consisting in the Montello thrust (Fantoni et al., 2002; Galadini et al., 2005). The Montello hill (Fig. 1) is generally interpreted as an actively growing ramp anticline on top of the north dipping thrust that has migrated south of the mountain into the foreland (Serpelloni et al., 2016).

The main geomorphological feature of the area is the presence of the NE-SW oriented Belluno Valley, where the Piave river flows, bounded to the north by the Dolomites and to the south by the Monte Grappa massif, the Monte Cesen-Col Visentin (MCCV) mountain chain and the Alpago-Cansiglio plateau (see Fig. 1). The MCCV is the morphological expression of an anticline associated with the BVT and back-thrust system, and it is crossed by the Piave river that flows to the southeast reaching the Montello hill. Highly productive fissured, hydrologically independent, karst aquifers are present in the area (Fig. 3; Filippini et al., 2018): in the Dolomites, one associated with the MCCV and one with the Alpago-Cansiglio plateau.

We find a strong temporal correlation between groundwater level changes in the Belluno

Valley, estimated from hydrological modeling, geodetic transient horizontal displacements and seismicity rates. We link hydrology to crustal deformation and geological structures by adopting physically-based models constrained by precipitation, temperature and river flow data and subsurface geological information; then, we show how water collected in a ~1000 km^2 basin focuses groundwater fluxes and pressure changes in a relatively narrow geological structure, generating transient horizontal deformation and perturbations of crustal stress of up to 25 kPa at seismogenic depths, modulating seismicity.

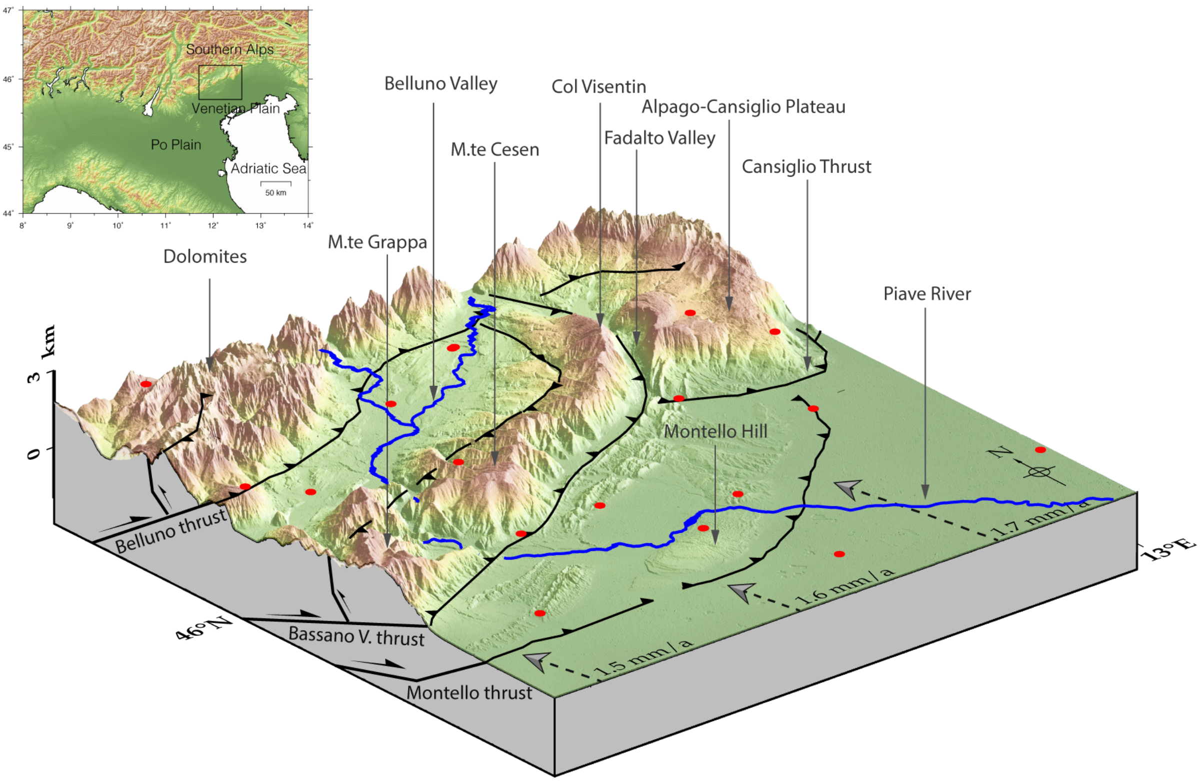

Figure 1. 3D view (from SW) of the study area. The dashed arrows indicate the Adria-Eurasia convergence rate and direction, predicted from a GNSS-derived rotation pole (Serpelloni et al., 2016). The digital elevation model, with topographic exaggeration, is obtained from ALOS Global Digital Surface Model data. The black lines represent the major fault lines. The red dots indicate the position of the GPS stations.

2. GNSS data and time-series analysis

Displacement time-series from GNSS stations in the 2010.0-2019.3 time span (Fig. 2 and Supplementary Figure S1.1), obtained following the procedures described in the Supplementary material (S1.1), have been analyzed with a blind source separation algorithm based on variational Bayesian Independent Component Analysis (vbICA; Gualandi et al., 2016). This approach, which uses a generative model to recreate the observations, allows extracting the spatiotemporal information of independent sources of deformation without imposing any specific spatial distribution or temporal function but extracting them directly from the observations, and it has been successfully used to extract hydrological and tectonic transient signals from GNSS displacements time series (Gualandi et al., 2017a; Gualandi et al., 2017b; Serpelloni et al., 2018).

The output of this analysis is the definition of a limited number of sources, or components, characterized by a specific spatial distribution (U) and following a specific temporal evolution (V). A weight coefficient S (in mm) is necessary to rescale their contribution in explaining the original data. Each independent component (IC) is described by a mix of Gaussians, which allows for more flexibility in the description of the sources with respect to classical independent component analysis (ICA) techniques. It allows to consistently take into account missing data in the data set (Chan et al., 2003) and provides an estimate of the uncertainty associated with each IC. The displacement time series at a given station can be reconstructed by linearly summing up the contributions from all the ICs, each of which is obtained by multiplying the specific spatial distribution by the associated weight times the temporal evolution.

With the goal of reducing the correlation of the dataset, making the search of the IC direction easier (Gualandi et al., 2016), the original time series are initially detrended. Differently from previous works using this approach, the trend of each GPS station is estimated in a multivariate statistical manner, by applying a vbICA analysis on displacement-time series realized in a Adria-fixed reference frame, as described in the Supplementary material S1.2. This approach is effective in removing the linear trend in case of strong non-linear signals and short time-series.

Once detrended, according to the F-test, 3 ICs are necessary to satisfactorily reconstruct the observed displacements. The temporal evolution (V) and spatial responses (U) of the three ICs are shown in Fig. 2. Seasonal annual displacements in the vertical and NS directions (IC1 and IC3) occur in response to surface hydrological mass loading (Serpelloni et al., 2018). A non-seasonal, horizontal transient deformation signal (IC2, Fig. 2), characterized by spatially variable amplitudes and directions, causes GNSS stations to reverse the sense of movement with time, resulting in a sequence of dilatational and compressional deformation oriented about normal to the mountain front.

Serpelloni et al. (2018) found that the temporal evolution of this signal correlates, somehow, with the history of cumulated precipitations at monthly timescales. Nonetheless, the link between surface deformation and changes in groundwater content remains difficult to find, because of the lack of water wells in the mountainous area and because of the limited spatial extent of the area affected by this transient deformation. Equivalent water content estimated from GRACE can provide only coarse spatial (Famiglietti et al., 2011) and temporal resolution for this area (Supplementary material S2.4).

In the next section we will use a lumped parameter hydrological mode to estimate daily changes of continental water content to be compared with the temporal evolution of IC2.

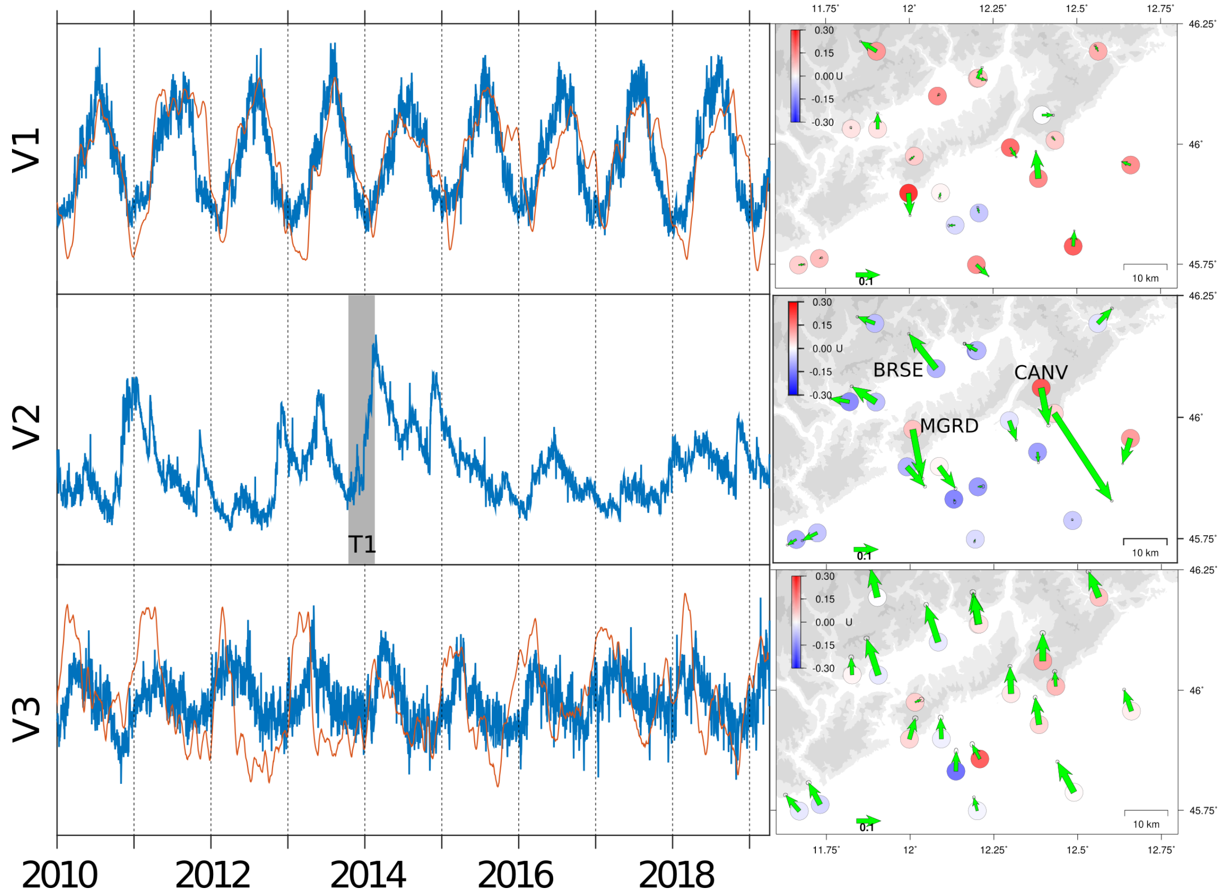

Figure 2. Temporal evolution (V; in blue) of the three ICs defined from the vbICA analysis and the corresponding spatial response in the horizontal (green arrows) and vertical (coloured circles) components, respectively. The gray area indicates the time interval (T1 = October 10th, 2013 - February 22nd, 2014) for which ground displacements have been computed and shown in Fig. 3. The red lines superimposed to V1 and V3 represent the mean vertical and N-S displacements caused by surface mass loading, respectively, estimated from the ERA-interim (European Centre for Medium-Range Weather Forecasts, ECMWF reanalysis) model and provided by http://loading.u-strasbg.fr (Gegout et al., 2010).

3. Surface deformation and link with hydrology

Water redistribution on the continents implies several processes that cover a wide range of spatial and temporal scales. At scales larger than several hundreds of kilometers, GRACE satellite observations or land surface models, such as the GLDAS modeling platform (Rodell et al., 2004), can provide a fair estimate of total water storage (TWS) changes and are typically used to compute surface displacements (Craig et al., 2017). At local scale, ground observations such as soil moisture and groundwater head can describe storage and pore-pressure changes, but their spatial representativity is limited. At regional/meso-scale, water storage observations are rare. River discharge, for example, is representative over the drained area (i.e. catchment), but only represents one flux contributing to storage changes. In this work, we consider a modeling approach to define meso-scale water storage changes, which is driven by meteorological river discharge observations.

Water storage changes in a downstream sub-catchment (see Fig. S2.1 in the Supplementary material) can be estimated based on the mass balance equation:

$$dS/dt = P + Qin - E - Qout - Qgw \quad (1)$$

where P, E, Qin, Qout, Qgw are respectively precipitation, actual evapotranspiration, incoming river inflow, outcoming river discharge, and potential groundwater import/export in a surrounding basin. Among the different water fluxes, P, Qin and Qout can be measured, while actual evapotranspiration and Qgw should be estimated with a model. It is worth noting that at regional scales (<100 km), lateral water fluxes could be significant, especially in a mountainous region, where the convergence of water from steep basins to valleys with gentle slopes favour transient accumulation of large amount of water. Such lateral flow processes are hardly modeled within large-scale hydrological models.

The tool we use to estimate the right side factors of eq. 1 is the lumped parameter hydrological model GR5J (Pushpalatha et al., 2011), which finally allow us to quantify daily TWS changes at the scale of single hydrological basins (Fig. 3). The GR5J rainfall-runoff model is based on two storage compartments, which mimic the typical response of soils and groundwater to antecedent precipitation. This model is forced with precipitation, temperature and potential evapotranspiration and computes actual river discharge. It is typically calibrated on observed river discharge to define the eight mathematical parameters defining the dynamics of the two stores and their relations. The best set of parameters values is then defined by a Marquard-Levenberg least squares regression analysis using root mean square error on the logarithm of discharge as an objective function. As discharge vary over two orders of magnitude, calibrating the model on the logarithm of the discharge is preferred to ensure that both high and low flows have a similar weight. In the end, total water storage changes is computed as the sum of both stores.

Since the GR5J inputs are a daily value of precipitation, temperature and potential evapotranspiration, we estimate the precipitation and temperature value form January 1st, 2010 to March 31st, 2019 by computing a daily weighted mean of in-situ observations managed by ARPAV (http://www.arpa.veneto.it/bollettini/storico), using the Thiessen polygon method (Supplementary material S2.1). Potential evapotranspiration has been evaluated by using the Jensen-Haise method (Jensen et al., 1990; Supplementary material S2.2).

In the study area we define three hydrological basins by using the drainage direction maps available on *www.hydrosheds.org/page/availability* and watershed outlets located at the river discharge measurements on the Piave river at Belluno, Segusino and of the Cordevole river at Ponte Mas (see Fig. 3). The region of interest, though, is limited to a portion of a watershed located in the Belluno Valley. Considering the availability of river discharge data upstream and downstream this region, the model is calibrated and water storage changes computed on each of the watershed (Supplementary material S2.3). The final TWS_{res} is set as the storage difference between the largest basin (Piave at Segusino) and its subbasins (Cordevole at Ponte Mas and the Piave at Belluno) as

$$TWS_{res}=TWS_{seg}-(TWS_{cor}+TWS_{bel}) \qquad (2)$$

Where TWS_{seg}, TWS_{cor}, TWS_{bel} indicate the TWS computed in the Piave at Segusino, Cordevole at Ponte Mas and Piave at Belluno watersheds, respectively.

Fig. 4 shows that the normalized temporal evolution of the non-seasonal deformation signal (V2) and TWS_{res} are clearly correlated (Pearson correlation coefficient = 0.83), demonstrating that this transient deformation component is driven by changes in groundwater contents. The agreement is good both during (rapid) TWS_{res} increase and (slower) TWS_{res} decrease, either when small and/or slow TWS_{res} changes happen and during extreme events. This process is also displayed in the Supplementary material V1.

On October 29th, 2018, storm Vaia, with >300 mm of cumulative precipitation in 72 hours and wind gusts exceeding 200 km/h, hit north-eastern Italy, causing the loss of 8 million cubic meters of standing trees. This extreme event is well recorded as a rapid increase of TWS_{res} (dashed line in Fig. 4) corresponding to extensional deformation recorded by the GNSS network, with the largest offsets at MGRD (~5 mm toward SE) and BRSE (~2.5 mm toward NW).

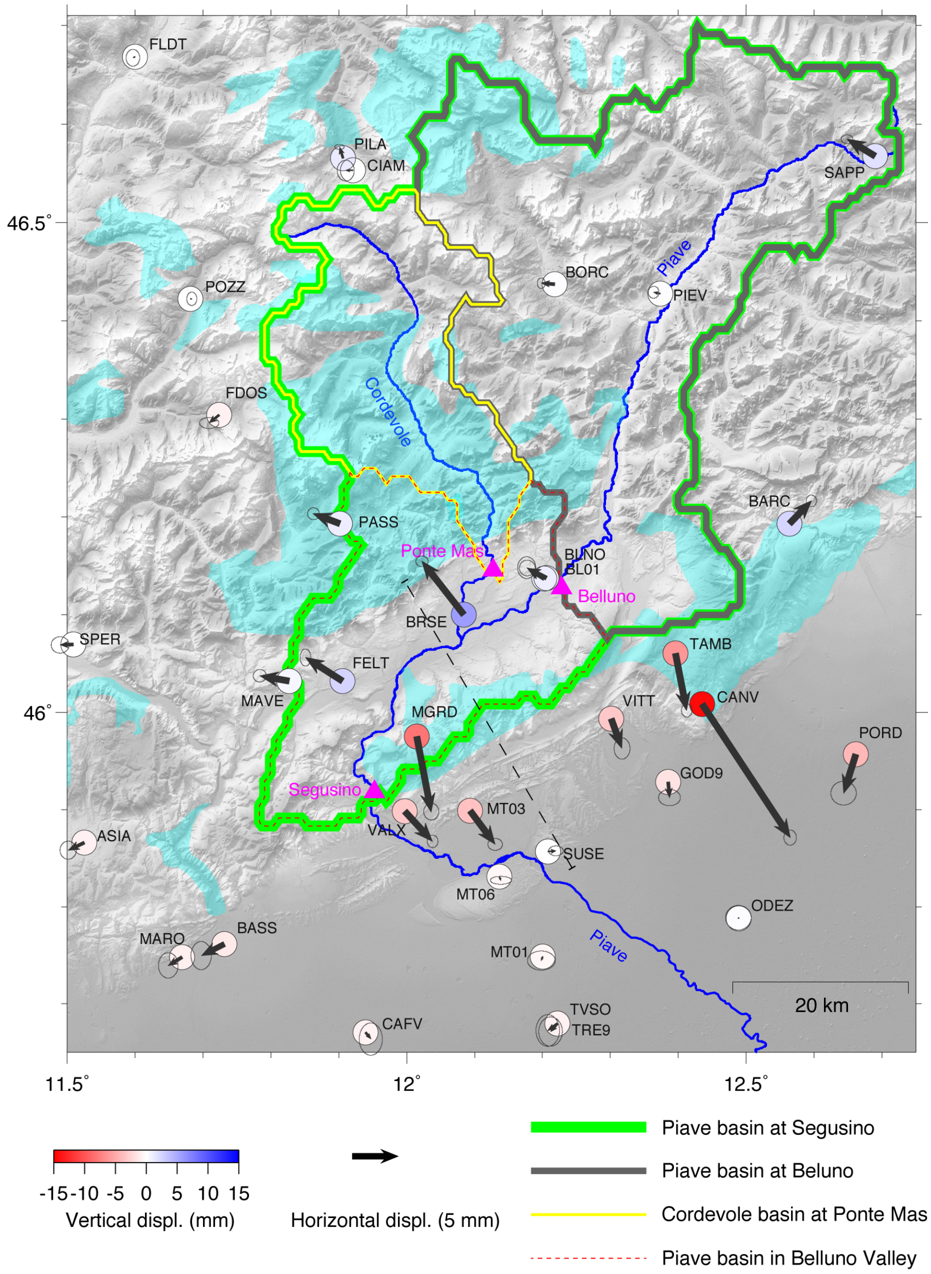

Figure 3. Hydrological map and geodetic displacements in the study region. Piave and Cordevole rivers (in blue) are gauged at three locations (purple triangles), defining three watersheds (yellow, green and grey) and the 883 km² region in-between (Belluno Valley, red dashed line) where water storage changes are modeled. Highly productive fissured karst aquifers are highlighted in cyan from the International Hydrogeological Map of Europe 1:1,500,000 (http://www.bgr.bund.de/ihme1500). Regional horizontal (black arrows) and vertical displacements (color dots), described by the second source of independent component analysis (IC2) on 67 GNSS stations during T1 period (winter 2013-2014) are superimposed (see also Fig. 2). The dashed black line show the trace of the geological cross section of Fig. 5.

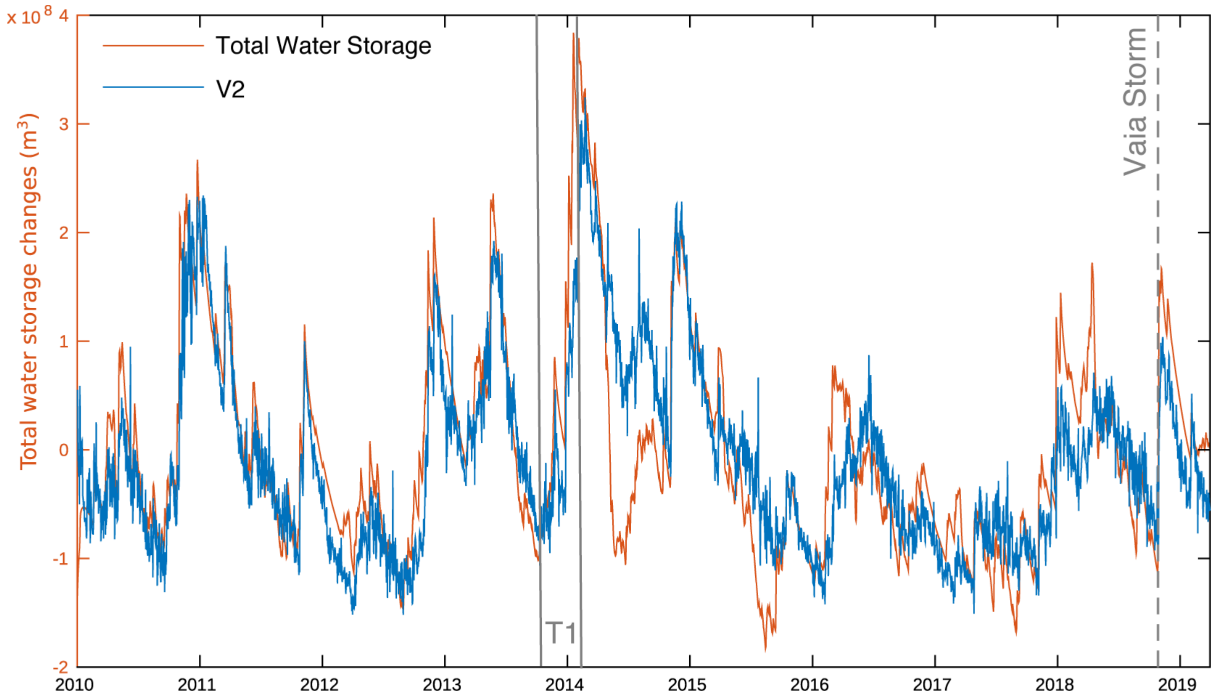

Figure 4. Temporal evolution of the modeled water storage changes in the Belluno Valley (orange, left axis) and the geodetic IC2 (blue). The vertical black lines indicate the T1 period and the epoch of the intense Vaia storm (dashed).

4. Surface deformation and link with geology

Transient displacements in the Alps have been interpreted as due to pressure changes associated with water level variations in vertical karst fractures (Devoti et al., 2015; Serpelloni et al., 2018). In this work we develop a two-dimensional finite-element model (FEM) with the goal of testing different sources of deformation potentially able to "accommodate" groundwater level changes in the Belluno Valley, comparing model results with the ground displacement pattern associated with the hydrological deformation component (Fig. 2). We use the "Solid Mechanics" physics module of the COMSOL software (Supplementary material S3.1), considering the problem as quasi-static at daily time scales and resolving the model as "stationary". We built the 2D model on the basis of the geological cross-section proposed by Galadini et al. (2005) (the trace of the cross section is shown in Fig. 3), which is constrained by geological and geophysical information, and is in agreement with local seismicity (Danesi et al., 2015; Romano et al., 2019) and seismic prospections (Fantoni et al., 2002). The cross section is normal to the strike of the MCCV mountain range, that is about parallel to the directions of geodetic displacements associated with IC2 (Fig. 2). We considered the GNSS stations located within 20 km from that cross section (considering a length of ~40 km of the Belluno Valley), whose positions and displacements are projected along the direction of the profile (Fig. 5). We focus on a specific time interval (October 10th, 2013 - February 22nd, 2014; T1 in Fig. 2 and Fig. 4), corresponding with a period of rapid increase of TWS_{res} and extensional deformation (Fig. 2).

The FEM model allows us to account for topography and subsurface geological features of the area, in particular the presence of faults and the different mechanical properties of the rock layers. The rock mechanical parameters used (Supplementary Table S3.1), in particular the Young modulus and Poisson's ratio, are taken from Anselmi et al. (2011).

The different models we tested to describe the relation between TWS_{res} changes and the deformation associated with IC2 (Fig. 6) are based on the assumption that the pressure variations caused by the accumulation of water are directly proportional to the TWS_{res} changes. We consider two main families of water pressure distribution:

1) models where pressure is distributed horizontally and applied vertically on the elastic domain: the loading caused by water storage changes in an unconfined aquifer, hosted by the Belluno Basin Units, cause a downward pressure on the aquiclude (impermeable layer, here the Igne Formation) at the base of the aquifer (Model 1). We also take into account the possible role of the Bassano-Valdobbiadene backthrust (BVBT) and BVT faults as lateral aquiclude (Model 2). In Model 3 we represent the surface loading on the Belluno Valley, assuming storage changes in a very shallow water reservoir, localized along the Piave river bed.

2) models where pressure is distributed vertically along sub-vertical structures and applied orthogonally in the modeled domain: Model 4, 5 mimic the impact of pressure changes in a

single open fracture reaching the surface, which represents the network of fractured rocks in the damage-zone associated with the BVT and the BVBT faults, respectively. Fault damage zones in the carbonate rocks, in fact, are often host to open fractures (karst), demonstrating that they can also be conductive to fluid flow (Torabi et al., 2019). Transient pressure changes are applied on the whole fracture, following Longuevergne et al. (2009). Such behavior has been validated in fractured karstic systems in Lesparre et al. (2017).

We use two criteria to evaluate how well a model reproduce the displacements pattern associated with IC2 (Figure S3.3). The first is the ratio between vertical and horizontal displacement at each GNSS station, which should not significantly exceed 1; the second is the number of stations with the horizontal displacements pattern in agreement in sign with IC2. According to these criteria, the displacements pattern associated with IC2 is better reproduced by the models where pressure is distributed vertically than the ones where pressure is distributed horizontally. In fact the vertical displacements generated by the Models 1, 2 and 3 are too large compared to the horizontal ones, and the horizontal displacements pattern shows significant disagreement with the one associated with IC2 (Fig. 2). A detailed analysis of each tested model, in terms of fit of the horizontal and vertical displacements, can be found in the Supplementary material S3.2.

The model that best reproduces the horizontal and vertical displacements is Model 5 in Fig, 6. Here the fracture is considered hydrologically conductive (Faulkner et al., 2010) down to 0 m a.s.l where it intersects an impermeable formation (the Igne Formation), as we will discuss in section 6.1.

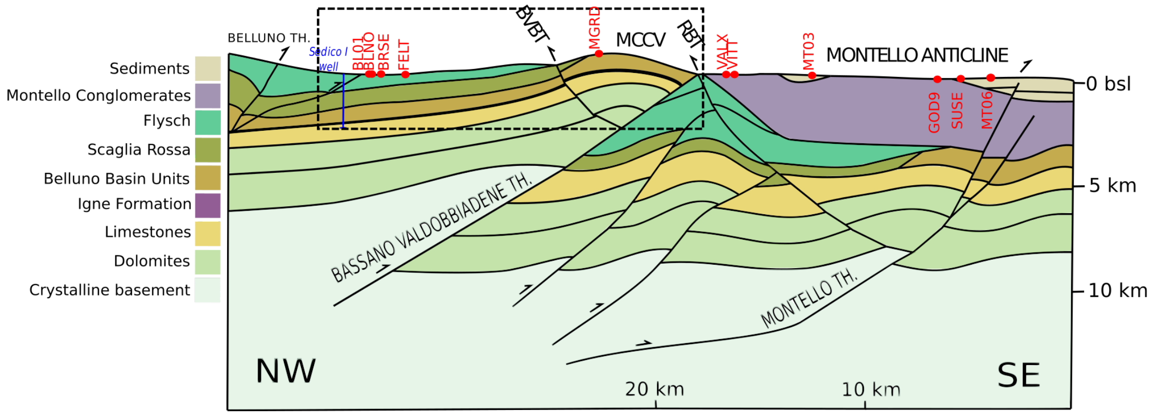

Figure 5. Geological cross section of the study area, modified from (Galadini et al., 2005); red dots: position of the GPS stations projected along this profile. RBT: Revine backthrust; BVBT: Bassano-Valdobbiadene back thrust. The dashed rectangle represents the area shown in Fig. 6.

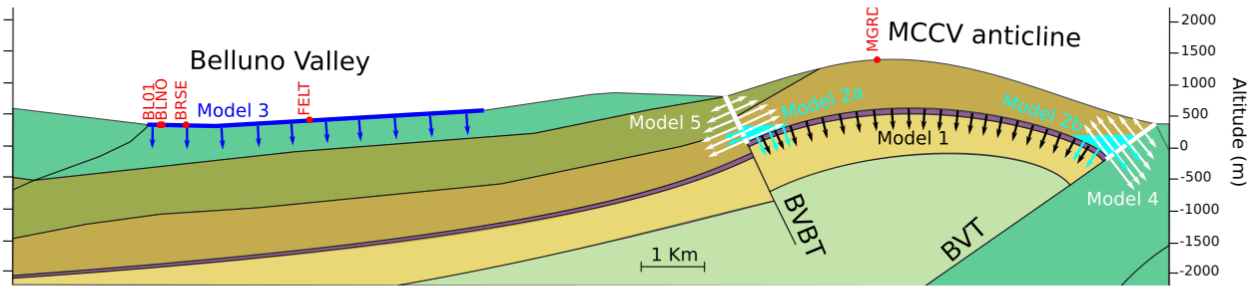

Figure 6. Zoom on the 2D model cross-section of Fig. 5, showing a schematic representation of the tested models used to explain the horizontal displacements reconstructed by IC2. MCCV: Mount Cesen-Col Visentin anticline; BVT: Bassano-Valdobbiadene thrust; BVBT: Bassano-Valdobbiadene backthrust. Rock formations are shown with the same legend of Fig. 5.

5. Hydrological control of seismicity

In Section 3 we demonstrate the link between hydrology and surface deformation (Fig. 3) and in Section 4 we provide a physical model explaining this process. In this section we investigate and test possible relationships between changes in TWS_{res} and seismicity rates. We use the local earthquake catalogue from Romano et al. (2019), which contains high-resolution relocations of events with magnitudes ranging from -0.8 to 4.5, in the period January 2012 to October 2017. This catalog was produced using data from the Collalto Seismic Network (Priolo et al., 2015).

Before exploring any possible link between seismicity rates and hydrological data, we identify and remove the aftershock events that are more likely associated with earthquake stress triggering processes. This analysis is performed by declustering the catalog in the time domain using the epidemic-type aftershock sequences model ETAS (Ogata, 1998). The resulting partition between background seismicity and aftershocks is presented in Fig. 7a. More details of this process are presented in the Supplementary material S4.1.

It is worth noting that in the ETAS model the background seismicity is assumed to be generated by a homogeneous Poisson process and is physically associated with a constant-rate tectonic loading process. However, the ETAS-based declustering process does not guarantees that the resulting background seismicity is actually stationary (Console et al., 2010), as a result it is actually possible to observe temporal fluctuations in the background seismicity obtained after the temporal declustering process. This departure from stationarity is supposed to be caused by the temporal activation or quiescence of seismic sources forced as a result of processes having a physical cause outside the stationary tectonic loading assumed by ETAS (Zhuang et al., 2002).

In this paper we explore possible correlations between temporal variations in hydrological data and the background seismicity. With this aim, we adopt the covariate model proposed by Garcia-Aristizabal (2018), which allows us to perform a robust statistical evaluation of possible relationships between TWS_{res} changes (x_{TWS}) and background seismicity rates. According to this model, when the forcing process generating the seismicity in a given zone is stationary in time (as e.g., a constant tectonic loading), the background seismicity rates can be stochastically modelled using a homogeneous Poisson process; it implies that seismicity rates follow the Poisson distribution and, consequently, the times between consecutive events (inter-event times, t_{IET}) follow the exponential distribution. However, if the forcing process is non-stationary, and if it is possible to identify measurable parameters as *proxies* of the processes driving such non stationary behavior, then it is possible to model correlations between changes in seismicity rates and changes in the proxy parameters by linking them as covariates of the stochastic model parameters. In order to explore this possibility we set the exponential distribution as the basic template function for modelling the distribution of t_{IET}:

$$f(t_{IET}|\mu(x_{TWS}))=\frac{1}{\mu(x_{TWS})}\exp\left(\frac{-t_{IET}}{\mu(x_{TWS})}\right) \tag{3}$$

and the possible dependencies on hydrological data (in this case x_{TWS}) are modelled writing the μ parameter of the exponential distribution in terms of deterministic functions of x_{TWS} of the explanatory covariate (Supplementary material S4.3). x_{TWS} is measured respect to a reference TWS_{res} assumed to be the minimum value reached by this parameter in the analysed period. In practice, we test polynomial functions relating $\log(\mu)$ and x_{TWS} as follows:

$$\log[\mu(x_{TWS})]=\sum_{j=0}^{n}\alpha_j(x_{TWS})^j \tag{4}$$

where α_j= ($\alpha_1,\alpha_2,\ldots,\alpha_n$) is a vector of coefficients of the polynomial function relating the μ parameter of the exponential distribution with the selected covariate x_{TWS}. We study in particular two competing models: the case $n=0$ represents a stationary model (i.e., non dependence on x_{TWS}), whereas the case $n=1$ represents a log-linear relationship (that is, an exponential relationship between μ and x_{TWS}). The input data are pairs of t_{IET} and the respective x_{TWS} averaged in a Δt time window (for which we test different values ranging from days to weeks). The inference of model parameter values is performed using a Markov chain Monte Carlo method, and the selection of the preferred model is performed calculating the Bayes factor (Garcia-Aristizabal, 2018). A more detailed description of this model is presented in the Supplementary material S4.3.

When considering the whole catalog of background seismicity (Supplementary Figure S4.2), the Bayes factor indicates that there is not significant evidence to support a non stationary model (Supplementary Table S4.2 and S4.3). However, the area covered by the earthquake catalogue is characterized by different active faults systems and we hypothesize that these fault systems could exhibit different responses to eventual stress perturbations related to hydrology. A visual inspection of the earthquake locations (Fig. 7a) allows us to note a high concentration of event locations in the NE part of the domain, whereas the seismicity towards the SW part of the domain tends to be more evenly distributed.

To quantitatively identify possible spatial sets of seismicity we implement a cluster analysis in the spatial domain (Supplementary material S4.2) using the k-means algorithm (MacQueen, 1967); the optimum cluster partition is selected using the Silhouette approach (Rousseeuw, 1987). We find that the background seismicity can be partitioned into two main clusters (Fig. 7b): (i) cluster A (orange points), located in the SW part of the domain, where earthquakes can be associated with the Montello thrust and the BVT faults (Danesi et al., 2015); (ii) cluster B (blue points), located in the NE part of the domain, in which most of the seismicity can be associated with the N-dipping Cansiglio thrust fault (Galadini et al., 2005; Fig. 1b). This preferential cluster partitioning roughly reflects the two main features that we observed in the spatial distribution of the seismicity: a set of events mostly grouped in the NE part, and a more evenly distributed seismicity towards the SW.

The correlation analysis using the covariate approach is then performed using the data from each spatial cluster of background seismicity. Comparing plots of the moving average of both TWS_{res} and the rate of seismic events (calculated in 90-days length time windows sliding at increments of 1 day) for cluster A (Fig. 8a) and cluster B (Fig. 8b), we observe that only the seismicity rate in cluster A tends to change in agreement with the changes in the TWS_{res}. This observation is quantitatively confirmed by the covariate analysis

(Supplementary material S4.3), with the Bayes factor indicating that only for cluster A the non stationary model performs better than the alternative stationary solution (Supplementary Table S4.3). In fact, for the cluster A (i.e., the seismicity associated with the Montello thrust and the BVT faults) there is positive evidence supporting a log-linear relationship between the seismicity rate (modelled through the distribution of inter-event times, t_{IET}) and the TWS_{res} changes, in contrast to a stationary reference model (Fig. 8c). On the other hand, for cluster B the evidence supports the stationary model (Fig. 8d), indicating a not significant link between seismicity rates in the Cansiglio thrust fault zone and TWS_{res} changes in the Belluno Valley. The parameter values of the fitted models are summarized in the Supplementary Table S4.4.

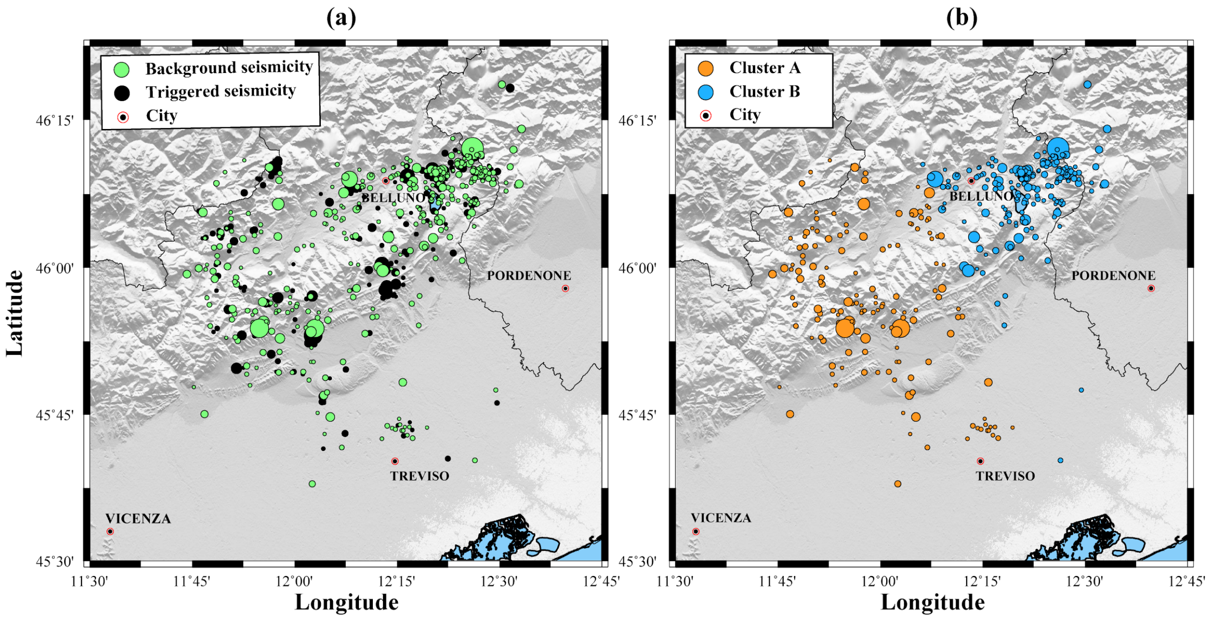

Figure 7. (a) Seismicity in the study area, separated as background (green circles) and triggered (black circles) seismicity according to the ETAS model. **(b)** Clusters (A and B) of background seismicity identified using spatial cluster analysis.

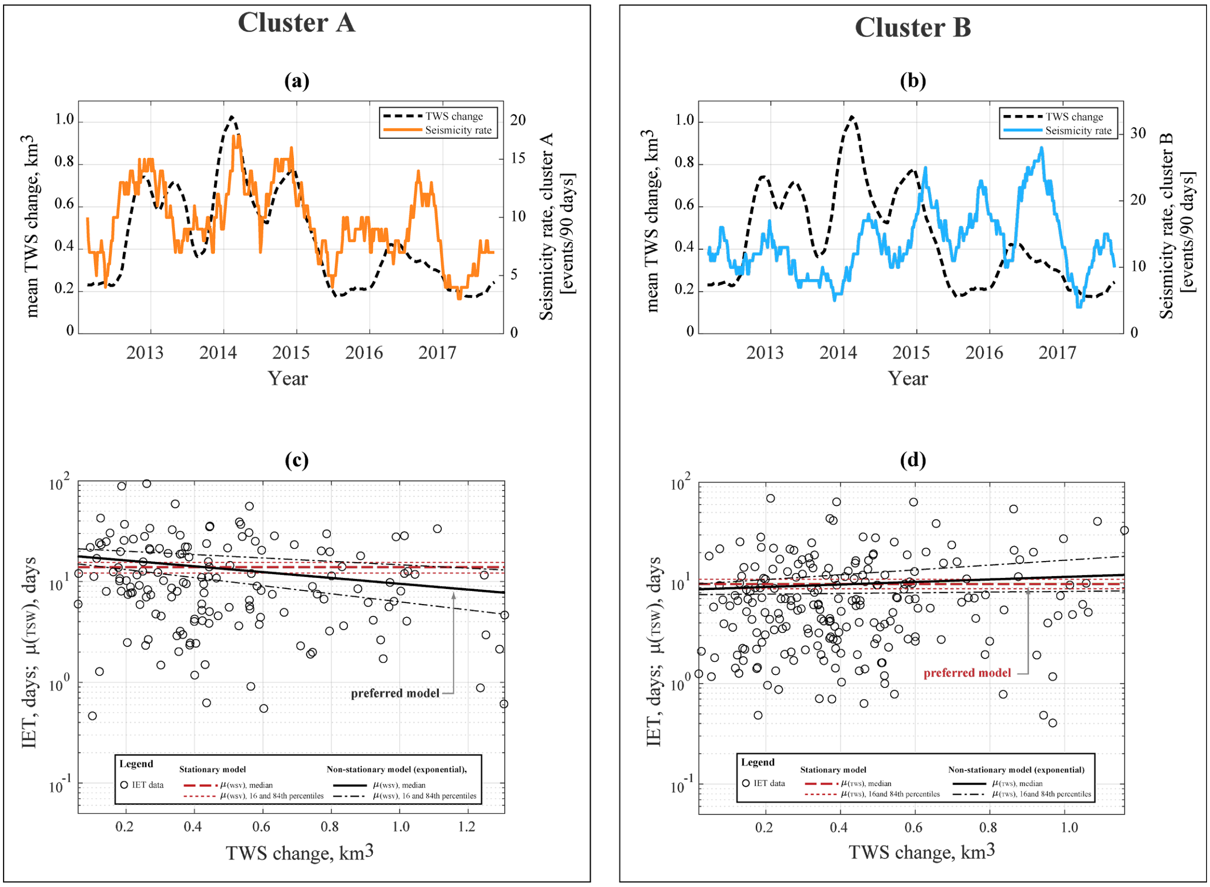

Figure 8. Moving average TWS (discontinuous black) and rate of seismic events in **(a)** cluster A (continuous orange) and **(b)** cluster B (continuous blue), calculated in 90-days length time windows sliding at increments of 1 day. Plot of inter-event times in **(c)** cluster A and **(d)** cluster B against TWS changes, and the results for the two tested models: stationary model (red) and Log-linear (black). Preferred models are indicated with the arrow in (c) (d).

6. Discussion

6.1 Hydromechanical coupling

In Sections 3 and 4 we described the link between hydrological processes and solid Earth deformation by the joint interpretation of hydrological and mechanical models results, constrained by geodetic, hydrological, meteorological observations and geological/geophysical information on subsurface structural and tectonic settings. We propose a possible mechanism able to explain water accumulation in a narrow, subvertical, geological structure and reproduce the horizontal anisotropic extensional deformation observed during a phase of large water storage increase. The same mechanism is assumed to be able to explain smaller deformation associated with phases of smaller TWS_{res} increase, and, with inverted sign, to explain the observed compressional deformation during phases of TWS_{res} decrease, responding to the fast dynamics of karst systems.

In our interpretation, we make the assumption that water level variations in rock fractures, or faults, are directly linked to the amount of water stored in the subsurface, which includes also water stored in the soil (i.e, soil moisture). However, the correlation between V2 and soil moisture values, as calculated from GLDAS Noah in the Piave at Segusino basin, is much lower (Pearson correlation coefficient = 0.18; see Figure S2.4 in the Supporting material) than the correlation between V2 and TWS_{res} (Pearson correlation coefficient = 0.83), suggesting that the greatest contribution to the measured transient geodetic displacements comes from groundwater, stored in karst rocks.

We assume that the network of damage-zone faults, which we model as a single fracture associated with BVBT in Model 5, are well connected and water-saturated; the water level varies as the TWS_{res}, causing pressure changes orthogonal to fracture walls. It is likely that the water feeding the fracture mainly comes from the top of the MCCV mountain chain: the higher fracture density at the hinge zone of the anticline (Feng and Gu, 2017) and the well-developed epikarst in the exposed rock formations (Maiolica and Rosso Ammonitico) suggest the presence of an epikarst circulation on the top of MCCV chain (Klimchouk and Sauro, 1996). The combined effect of the epikarst and the presence of a shallow, low permeable layer (the Fonzaso formation, located at ~200 m of depth from the surface) facilitates the rapid infiltration of precipitation water and its flow toward the backthrust, following the northward inclination of rock layers and stratification; this hypothesis is supported by the observed lack of a time-delay, at the daily time scale, between TWS_{res} and the geodetic deformation signal (Fig. 4). However, we can not exclude that water can flow southward, toward the BVT, which might behave similarly to the backthrust as an hydrologically active structure (Supplementary material S3.2, Model 4). Nonetheless, the site MGRD (Fig. 1a) moves toward the BVT and away from the backthrust when TWS_{res} increases, implying that an hydrologically active BVT is likely to have a secondary effect with respect to its backthrust.

A more precise description of the source of deformation, which includes the identification of both the fracture bottom position and the water level rise inside it, is not straightforward because of the trade-off between fracture width and its opening (e.g., Silverii et al., 2016; Devoti et al., 2015). Nonetheless, because of the lack of evidences of aquifers reaching depths that are hundreds of meters below the sea level surface, and since the maximum water level variation measured in a similar karst system is ~300 m (Milanovic, 2005), we assume the bottom position of the fracture at 0 m above sea level, at the interface between the Vajont limestone and the more impermeable Igne formation (see Fig. 6). Once set the bottom position of the fracture, the water level rise that provides the best match between modeled and observed displacements is 100 m (Fig. S3.3), with the water level inside the fracture located at about 10 m below the free surface when V2 reaches its maximum during the analyzed time-period (i.e., January, 2014). Furthermore, we analyze the effect of the initial opening of the fracture when applying the same pressure values on its walls; we have found that assuming different initial opening values does not impact significantly the resulting displacements (Fig. S3.4). It follows that it is not possible to quantify the volumes of water involved, since the only quantity affecting the displacements is the water level variation, while the initial fracture opening does not play a key role.

Although the 2D numerical model used is an acceptable simplification, given the spatial distribution and density of available geodetic data, we are aware of its limitations. We are assuming that geological features (including for example outcropping formations, fracture spacing, strike of faults and fractures, topography) are constant along the SW-NE direction, for about 40 km, which is not necessarily true. A 2D model cannot take into account the fact the the MCCV mountain chain and associated thrust and back thrust faults curve north, going into the Fadalto valley (see Fig. 1). More importantly, changes in water level along the backthrust are implicitly assumed to be uniform along its strike in a 2D model, but an heterogeneous change in water level can cause more localized deformation signals, which would be however difficult to detect with the present GNSS network configuration. Moreover, effects associated with similar processes occurring at nearby karst systems cannot be taken into consideration. Hydrological deformation in the Cansiglio plateau, in fact (Devoti et al., 2015; Serpelloni et al., 2018) may affect GNSS sites VITT and GOD9 (Fig. 1). Additional GNSS stations will be necessary to overcome these problems.

6.2 Seismotectonic implications

Two main mechanisms have been suggested to explain hydrological modulation of seismicity: variations in pore-fluid pressure at hypocentral depths (Hainzl et al., 2006) and direct stress on the fault plane (Bettinelli et al., 2008; Craig et al., 2017; Johnson et al., 2017; D'Agostino et al., 2018). In the latter case, there is usually a little or no time delay between hydrological indicators and seismicity rate. In the former, seismicity rate variations are usually delayed with respect to hydrological observations by a time lag, which is strictly dependent on the earthquake nucleation depth and on the hydraulic diffusivity of the material between the surface and the seismicity source. The lack of temporal delay between the seismicity rate and the TWS_{res} (Fig. 4) excludes an important role for poroelastic contributions, making direct effect of stress changes at seismogenic depths the most likely process linking hydrology and seismicity.

In case of seasonal stress perturbations, seismicity rates can correlate either with the stress values or with stress rates, depending if the period of the stress perturbation (T_p) is smaller or larger than a critical period (T_a), which in turn is controlled by the loading plate velocity (Ader et al., 2014). The period that dominates the temporal evolution of stress in the study area is 1 yr (Supplementary Figure S2.5), which is a value that $T_a$reaches only in rapidly deforming regions (Bettinelli et al., 2008). In slowly deforming regions, as the Southern Alps, T_a usually assumes larger values. This observation is consistent with our findings, implying that stress changes are proportional to the magnitude of the TWS_{res} and not to its time derivative (which represents whether TWS_{res} is in an increasing or decreasing phase).

We estimate the stress change associated with the deformation caused by the water pressure increase (T1 time window in Fig. 4) in the hypothesized fracture source. In practice, we calculate the Coulomb failure function (CFF, Supplementary material S3.3) on receiving planes oriented in agreement with the compressional tectonic regime of the area. Fig. 9a shows CFF values assuming a shallow-dipping (10°) decollement (i.e. the Montello flat) as receiving source, showing that in the depth interval where most of the seismicity associated with cluster A (see Fig. 7b) is located (4-14 km), positive stress changes are up to 25 KPa. These stress changes are larger than stressing rates from tectonic loading, which are expected to be of the order of 1-3 KPa (Caporali et al., 2018). Similar values are obtained, but with different spatial patterns, assuming different thrust-receiving sources; however, a correlation between areas of stress increase and seismicity is not evident. Unfortunately, the faulting mechanisms of the background seismicity are not well constrained, and the focal mechanisms available for other events in the catalogue (Romano et al., 2019) show a large range of mechanisms, including normal, thrust and strike-slip faulting on different planes. So, while a clear spatial correlation between seismicity and regions of positive stress increase is not apparent, it is likely that the highly deformed upper crust, inherited by the complex tectonic evolution of the Southern Alps (Castellarin and Cantelli, 2000), provides heterogeneous response to the hydrologically-modulated stress changes.

It is however important to note that the amplitude of the CFF field generated by the TWS_{res} increase in hydrologically active fracture is much larger than the one generated by the annual surface hydrological mass loading (Fig. 9b), which actually is considered as the main mechanisms that modulate seismicity rates in other regions (Hainzl et al., 2014; Johnson et al., 2017), where, however, much greater annual vertical displacements, and consequently greater seasonal stress perturbations than those observed in the Alps, are present.

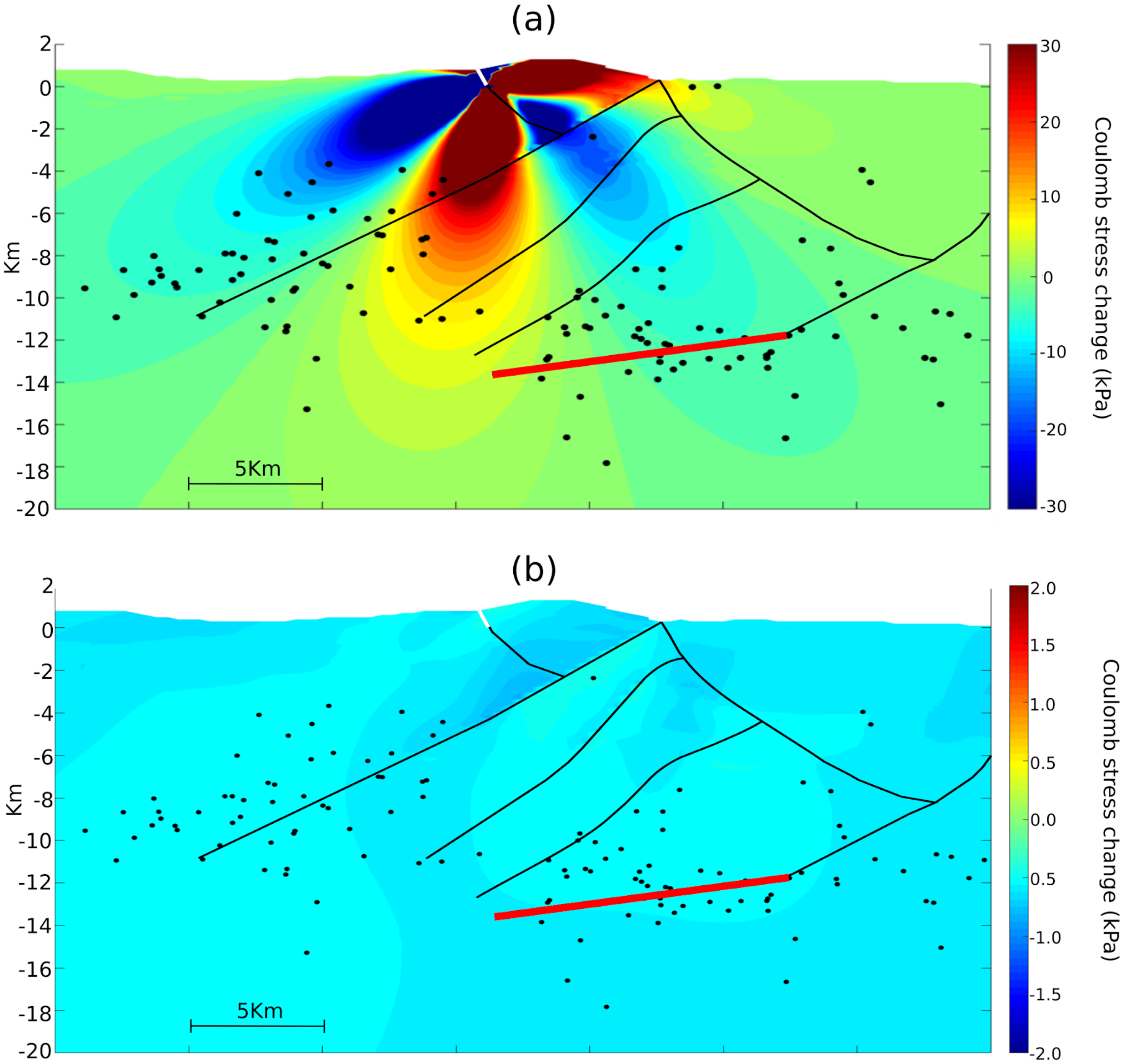

Figure 9. (a) Coulomb stress change during a phase of TWS_{res} increase (T1 in Fig. 4) caused by a source of deformation as in Model 5 (see Supplementary material S3.2), considering planes parallel to the Montello decollement (dip angle=10°), highlighted in red. **(b)** Coulomb stress change calculated on the same dipping planes considering as source of deformation a 1 kPa uniform load on the free surface. This value causes a subsidence of ~3.8 mm, which is consistent with the amplitude of the vertical displacements caused by the large scale superficial loading in the time interval that goes from summer to winter (see Fig. 2) and inhibits thrust faulting (negative CFF values in all the domain). The black dots represent the background seismicity of cluster A.

7. Conclusions

Using geodetic, hydrological and meteorological data, integrated into hydrological and mechanical models, we show how water converging from a large drainage area (~1000 km²) toward a specific zone, can generate horizontal surface displacements that are superimposed to surface hydrological and tectonic loading. Our results demonstrate that hydrologically-active and seismically-active faults can be totally disconnected, and that stress transfer is a critical mechanism for triggering seismicity at depths reaching more than 10 km below the surface. We show that hydraulic pressure changes in a shallow fracture (<1 km) can generate large shears (~10 kPa) in faults oriented orthogonally and at distances of the order of ~10 km (horizontally and vertically). In such a context, the link between hydrology and seismicity is favoured by 1) the existence of a (shallow) hydrologically-active fracture connected to the surface; 2) the existence of properly oriented (orthogonal), seismically active structures (such as a classical thrust/backthrust couple), and 3) water convergence from a watershed/river basin towards the hydrologically active structure, leading to large water storage (and therefore water pressure) changes. In such contexts, horizontal deformation is best suited to highlight physical links between surface deformation and hydro-mechanical processes occurring at depth.

Acknowledgements

We thank L. Anderlini for helpful discussions and suggestions on stress analysis and E. Scoccimarro for suggestion on the analysis of pluviometric data.

Author contributions

F.P. conceived and led the paper and performed numerical and hydrological modeling. E.S. coordinated the study and analyzed GNSS data. L.L. supervised hydrological modeling and interpretation. A.G.A and L.F. performed the analysis of the earthquake catalogue. M.E.B.

cross-examined the results and supervised F.P. PhD. A.G. supervised the analysis of GNSS displacements. L.D. supported hydro-geological interpretation. F.P., E.S., L.L., A.G.A. and L.F wrote the paper. All the authors discussed the content of the paper and shared the writing.

Competing interests

The authors declare no competing interests.

Data availability

Precipitation, temperature and river flow data are provided by “Agenzia Regionale per la Prevenzione e Protezione Ambientale del Veneto” (ARPAV): https://www.arpa.veneto.it/bollettini/storico/Mappa_2019_TEMP.htm.

Extraterrestrial irradiance data are available from http://www.soda-pro.com/web-services/radiation/extraterrestrial-irradiance-and-toa.

Drainage direction maps used to define river basins are available on *www.hydrosheds.org/page/availability*.

The analyzed seismic catalog is available in the supplementary material of Romano et al. (2019).

We use publicly available raw GNSS data. However, RINEX data can be requested to E.S., if not yet available on the original repositories.

Raw GPS time series are available on https://doi.org/10.1594/PANGAEA.912895

The Collalto Seismic Network data are available on https://doi.org/10.7914/SN/EV.

Code availability

The MATLAB code for TWS estimation and vbICA decomposition are available from the corresponding author on request.

Founding source

This work was supported by the project TRANSIENTI, founded by the Italian Ministry of Education, Universities and Research (MIUR) “Premiale 2014”.

References

Ader, T.J., Lapusta, N., Avouac, J.-P., Ampuero, J.-P., 2014. Response of rate-and-state seismogenic faults to harmonic shear-stress perturbations. Geophys. J. Int. 198, 385–413. doi:10.1093/gji/ggu144

Anderlini, L., Serpelloni, E., Tolomei, C., De Martini, P.M., Pezzo, G., Gualandi, A., Spada, G., 2020. New insights into active tectonics and seismogenic potential of the Italian Southern Alps from vertical geodetic velocities. doi:10.5194/se-2020-10

Anselmi, M., Govoni, A., De Gori, P., Chiarabba, C., 2011. Seismicity and velocity structures along the south-Alpine thrust front of the Venetian Alps (NE-Italy). Tectonophysics 513, 37–48. doi:10.1016/j.tecto.2011.09.023

Bettinelli, P., Avouac, J.-P., Flouzat, M., Bollinger, L., Ramillien, G., Rajaure, S., Sapkota, S., 2008. Seasonal variations of seismicity and geodetic strain in the Himalaya induced by surface hydrology. Earth and Planetary Science Letters 266, 332–344. doi:10.1016/j.epsl.2007.11.021

Borsa, A.A., Agnew, D.C., Cayan, D.R., 2014. Remote Hydrology. Ongoing drought-induced uplift in the western United States. Science 345, 1587–1590. doi:10.1126/science.1260279

Caporali, A., Braitenberg, C., Montone, P., Rossi, G., Valensise, G., Viganò, A., Zurutuza, J., 2018. A quantitative approach to the loading rate of seismogenic sources in Italy. Geophys. J. Int. 213, 2096–2111. doi:10.1093/gji/ggy112

Castellarin, A., Cantelli, L., 2000. Neo-Alpine evolution of the Southern Eastern Alps. Journal of Geodynamics 30, 251–274. doi:10.1016/S0264-3707(99)00036-8

Chanard, K., Avouac, J.P., Ramillien, G., Genrich, J., 2014. Modeling deformation induced by seasonal variations of continental water in the Himalaya region: Sensitivity to Earth elastic structure. J. Geophys. Res. Solid Earth 119, 5097–5113. doi:10.1002/2013JB010451

Chanard, K., Fleitout, L., Calais, E., Barbot, S., Avouac, J.-P., 2018. Constraints on transient viscoelastic rheology of the asthenosphere from seasonal deformation. Geophys. Res. Lett. 45, 2328–2338. doi:10.1002/2017GL076451

Chan, K., Lee, T.-W., Sejnowski, T.J., 2003. Variational Bayesian Learning of ICA with Missing Data. Neural Comput. 15, 1991–2011. doi:10.1162/08997660360675116

Console, R., Jackson, D.D., Kagan, Y.Y., 2010. Using the ETAS model for catalog declustering and seismic background assessment. Pure appl. geophys. 167, 819–830. doi:10.1007/s00024-010-0065-5

Craig, T.J., Chanard, K., Calais, E., 2017. Hydrologically-driven crustal stresses and seismicity in the New Madrid Seismic Zone. Nat. Commun. 8, 2143. doi:10.1038/s41467-017-01696-w

D'Agostino, N., Silverii, F., Amoroso, O., Convertito, V., Fiorillo, F., Ventafridda, G., Zollo, A., 2018. Crustal deformation and seismicity modulated by groundwater recharge of karst aquifers. Geophys. Res. Lett. 45, 12,253-12,262. doi:10.1029/2018GL079794

Danesi, S., Pondrelli, S., Salimbeni, S., Cavaliere, A., Serpelloni, E., Danecek, P., Lovati, S., Massa, M., 2015. Active deformation and seismicity in the Southern Alps (Italy): The Montello hill as a case study. Tectonophysics 653, 95–108. doi:10.1016/j.tecto.2015.03.028

Devoti, R., Riguzzi, F., Cinti, F.R., Ventura, G., 2018. Long-term strain oscillations related to the hydrological interaction between aquifers in intra-mountain basins: A case study from Apennines chain (Italy). Earth and Planetary Science Letters 501, 1–12. doi:10.1016/j.epsl.2018.08.014

Devoti, R., Zuliani, D., Braitenberg, C., Fabris, P., Grillo, B., 2015. Hydrologically induced slope deformations detected by GPS and clinometric surveys in the Cansiglio Plateau, southern Alps. Earth and Planetary Science Letters 419, 134–142. doi:10.1016/j.epsl.2015.03.023

Drouin, V., Heki, K., Sigmundsson, F., Hreinsdóttir, S., Ófeigsson, B.G., 2016. Constraints on seasonal load variations and regional rigidity from continuous GPS measurements in Iceland, 1997–2014. Geophys. J. Int. 205, 1843–1858. doi:10.1093/gji/ggw122

Famiglietti, J.S., Lo, M., Ho, S.L., Bethune, J., Anderson, K.J., Syed, T.H., Swenson, S.C., de Linage, C.R., Rodell, M., 2011. Satellites measure recent rates of groundwater depletion in California's Central Valley. Geophys. Res. Lett. 38. doi:10.1029/2010GL046442

Fantoni, R., Catellani, D., Merlini, S., Rogledi, S., Venturini, S., 2002. La registrazione degli eventi deformativi cenozoici nell'avampaese Veneto-Friulano. Mem. Soc. Geol. It 57, 301–313.

Faulkner, D.R., Jackson, C.A.L., Lunn, R.J., Schlische, R.W., Shipton, Z.K., Wibberley, C.A.J., Withjack, M.O., 2010. A review of recent developments concerning the structure, mechanics and fluid flow properties of fault zones. Journal of Structural Geology 32, 1557–1575. doi:10.1016/j.jsg.2010.06.009

Feng, J., Gu, K., 2017. Geomechanical Modeling of Stress and Fracture Distribution during Contractional Fault-Related Folding. GEP 05, 61–93. doi:10.4236/gep.2017.511006

Filippini, M., Squarzoni, G., De Waele, J., Fiorucci, A., Vigna, B., Grillo, B., Riva, A., Rossetti, S., Zini, L., Casagrande, G., Stumpp, C., Gargini, A., 2018. Differentiated spring behavior under changing hydrological conditions in an alpine karst aquifer. J Hydrol (Amst) 556, 572–584. doi:10.1016/j.jhydrol.2017.11.040

Fu, Y., Argus, D.F., Freymueller, J.T., Heflin, M.B., 2013. Horizontal motion in elastic response to seasonal loading of rain water in the Amazon Basin and monsoon water in Southeast Asia observed by GPS and inferred from GRACE. Geophys. Res. Lett. 40, 6048–6053. doi:10.1002/2013GL058093

Galadini, F., Poli, M.E., Zanferrari, A., 2005. Seismogenic sources potentially responsible for earthquakes with $M \geq 6$ in the eastern Southern Alps (Thiene-Udine sector, NE Italy). Geophys. J. Int. 161, 739–762. doi:10.1111/j.1365-246X.2005.02571.x

Garcia-Aristizabal, A., 2018. Modelling fluid-induced seismicity rates associated with fluid injections: examples related to fracture stimulations in geothermal areas. Geophys. J. Int. 215, 471–493. doi:10.1093/gji/ggy284

Gegout, P., Boy, J.P., Hinderer, J., Ferhat, G., 2010. Modeling and Observation of Loading Contribution to Time-Variable GPS Sites Positions, in: Mertikas, S.P. (Ed.), Gravity, Geoid and Earth Observation: IAG Commission 2: Gravity Field, Chania, Crete, Greece, 23-27 June 2008, International Association of Geodesy Symposia. Springer Berlin Heidelberg, Berlin, Heidelberg, pp. 651–659. doi:10.1007/978-3-642-10634-7_86

Gualandi, A., Nichele, C., Serpelloni, E., Chiaraluce, L., Anderlini, L., Latorre, D., Belardinelli, M.E., Avouac, J.P., 2017a. Aseismic deformation associated with an earthquake swarm in the northern Apennines (Italy). Geophys. Res. Lett. 44, 7706–7714. doi:10.1002/2017GL073687

Gualandi, A., Perfettini, H., Radiguet, M., Cotte, N., Kostoglodov, V., 2017b. GPS deformation related to the *M* 7.3, 2014, Papanoa earthquake (Mexico) reveals the aseismic behavior of the Guerrero seismic gap. Geophys. Res. Lett. 44, 6039–6047. doi:10.1002/2017GL072913

Gualandi, A., Serpelloni, E., Belardinelli, M.E., 2016. Blind source separation problem in GPS time series. J. Geod. 90, 323–341. doi:10.1007/s00190-015-0875-4

Hainzl, S., Aggarwal, S.K., Khan, P.K., Rastogi, B.K., 2014. Monsoon-induced earthquake activity in Talala, Gujarat, India. Geophys. J. Int. 200, 627–637. doi:10.1093/gji/ggu421

Hainzl, S., Kraft, T., Wassermann, J., Igel, H., Schmedes, E., 2006. Evidence for rainfall-triggered earthquake activity. Geophys. Res. Lett. 33. doi:10.1029/2006GL027642

Jensen, M.E., Burman, R.D., Allen, R.G., 1990. Evapotranspiration and irrigation water requirements.

Johnson, C.W., Fu, Y., Bürgmann, R., 2017. Seasonal water storage, stress modulation, and California seismicity. Science 356, 1161–1164. doi:10.1126/science.aak9547

Klimchouk, A.B., Sauro, U., 1996. Hidden’shafts at the base of the epikarstic zone: a case study from the Sette Communi plateau, Venetian Pre-Alps, Italy. Cave and karst science 23, 101–107.

Lesparre, N., Boudin, F., Champollion, C., Chéry, J., Danquigny, C., Seat, H.C., Cattoen, M., Lizion, F., Longuevergne, L., 2017. New insights on fractures deformation from tiltmeter data measured inside the Fontaine de Vaucluse karst system. Geophys. J. Int. 208, 1389–1402. doi:10.1093/gji/ggw446

Longuevergne, L., Florsch, N., Boudin, F., Oudin, L., Camerlynck, C., 2009. Tilt and strain deformation induced by hydrologically active natural fractures: application to the tiltmeters installed in Sainte-Croix-aux-Mines observatory (France). Geophys. J. Int. 178, 667–677. doi:10.1111/j.1365-246X.2009.04197.x

MacQueen, J., 1967. Some methods for classification and analysis of multivariate observations. Proceedings of the fifth Berkeley symposium on mathematical statistics and probability 1, 281–297.

Milanovic, P.T., 2005. Water resources engineering in karst.

Ogata, Y., 1998. Space-Time Point-Process Models for Earthquake Occurrences. Ann. Inst. Stat. Math. 50, 379–402. doi:10.1023/A:1003403601725

Priolo, E., Romanelli, M., Plasencia Linares, M.P., Garbin, M., Peruzza, L., Romano, M.A., Marotta, P., Bernardi, P., Moratto, L., Zuliani, D., Fabris, P., 2015. Seismic monitoring of an underground natural gas storage facility: the collalto seismic network. Seismological Research Letters 86, 109–123. doi:10.1785/0220140087

Pushpalatha, R., Perrin, C., Le Moine, N., Mathevet, T., Andréassian, V., 2011. A downward structural sensitivity analysis of hydrological models to improve low-flow simulation. J Hydrol (Amst) 411, 66–76. doi:10.1016/j.jhydrol.2011.09.034

Rodell, M., Houser, P.R., Jambor, U., Gottschalck, J., Mitchell, K., Meng, C.J., Arsenault, K., Cosgrove, B., Radakovich, J., Bosilovich, M., Entin, J.K., Walker, J.P., Lohmann, D., Toll, D., 2004. The global land data assimilation system. Bull. Amer. Meteor. Soc. 85, 381–394. doi:10.1175/BAMS-85-3-381

Romano, M.A., Peruzza, L., Garbin, M., Priolo, E., Picotti, V., 2019. Microseismic Portrait of the Montello Thrust (Southeastern Alps, Italy) from a Dense High-Quality Seismic Network. Seismological Research Letters. doi:10.1785/0220180387

Rousseeuw, P.J., 1987. Silhouettes: A graphical aid to the interpretation and validation of cluster analysis. Journal of Computational and Applied Mathematics 20, 53–65. doi:10.1016/0377-0427(87)90125-7

Serpelloni, E., Pintori, F., Gualandi, A., Scoccimarro, E., Cavaliere, A., Anderlini, L., Belardinelli, M.E., Todesco, M., 2018. Hydrologically Induced Karst Deformation: Insights From GPS Measurements in the Adria-Eurasia Plate Boundary Zone. J. Geophys. Res. Solid Earth 123, 4413–4430. doi:10.1002/2017JB015252

Serpelloni, E., Vannucci, G., Anderlini, L., Bennett, R.A., 2016. Kinematics, seismotectonics and seismic potential of the eastern sector of the European Alps from GPS and seismic deformation data. Tectonophysics 688, 157–181. doi:10.1016/j.tecto.2016.09.026

Silverii, F., D’Agostino, N., Métois, M., Fiorillo, F., Ventafridda, G., 2016. Transient deformation of karst aquifers due to seasonal and multiyear groundwater variations observed by GPS in southern Apennines (Italy). J. Geophys. Res. Solid Earth 121, 8315–8337. doi:10.1002/2016JB013361

Torabi, A., Ellingsen, T.S.S., Johannessen, M.U., Alaei, B., Rotevatn, A., Chiarella, D., 2019. Fault zone architecture and its scaling laws: where does the damage zone start and stop? Geological Society, London, Special Publications SP496-2018–151. doi:10.1144/SP496-2018-151

van Dam, T., Wahr, J., Milly, P.C.D., Shmakin, A.B., Blewitt, G., Lavallée, D., Larson, K.M., 2001. Crustal displacements due to continental water loading. Geophys. Res. Lett. 28, 651–654. doi:10.1029/2000GL012120

Zhuang, J., Ogata, Y., Vere-Jones, D., 2002. Stochastic Declustering of Space-Time Earthquake Occurrences. J. Am. Stat. Assoc. 97, 369–380. doi:10.1198/016214502760046925